Mechanism of inhibition of HIV-1 reverse transcriptase by non-nucleoside inhibitors

Robert Esnouf[1,2], Jingshan Ren[1], Carl Ross[3], Yvonne Jones[1,2], David Stammers[3] and David Stuart[1,2]

The structure of unliganded HIV-1 reverse transcriptase has been determined at 2.35 Å resolution and refined to an *R*-factor of 0.219 (for all data) with good stereochemistry. The unliganded structure was produced by soaking out a weak binding non-nucleoside inhibitor, HEPT, from pregrown crystals. Comparison with the structures of four different RT and non-nucleoside inhibitor complexes reveals that only minor domain rearrangements occur, but there is a significant repositioning of a three-stranded β-sheet in the p66 subunit (containing the catalytic aspartic acid residues 110, 185 and 186) with respect to the rest of the polymerase site. This suggests that NNIs inhibit RT by locking the polymerase active site in an inactive conformation, reminiscent of the conformation observed in the inactive p51 subunit.

[1]The Laboratory of Molecular Biophysics, Rex Richards Building, South Parks Road, Oxford, OX1 3QU, UK
[2]The Oxford Centre for Molecular Sciences, New Chemistry Building, South Parks Road, Oxford, OX1 3QT, UK
[3]Structural Biology Group, The Wellcome Research Laboratories, Langley Court, Beckenham, Kent, BR3 3BS, UK

Inhibitors of HIV reverse transcriptase are cornerstones in the treatment of AIDS patients. A number of nucleoside-analogue RT inhibitors including AZT, ddI and ddC have been approved for such use. The development of a wide variety of non-nucleoside analogue RT inhibitors (NNIs) has been the focus of much effort to find further treatments for AIDS. Amongst the first NNIs to be described were HEPT[1], TIBO[2] and nevirapine[3]. Since then a wide range of chemically diverse compounds with similar characteristics as inhibitors of RT have been described[4]. The common kinetic feature of these compounds is that they are highly selective for HIV-1 RT and generally are non-competitive inhibitors that appear to bind in a region close to the polymerase active site[5,6]. Crystallographic studies of nevirapine binding to RT reveal a site close to the conserved, catalytically important, aspartic acid residues (110, 185 and 186)[7–9]. Structures of complexes of RT with different NNIs reveal binding at a site in common with nevirapine and a high degree of spatial overlap for the different inhibitors[9]. Suggestions about the mechanism of the inhibition of RT by this class of compounds have included the idea that they attenuate the relative movement of domains within the RT heterodimer and also that they cause a distortion in the active site region[7,10]. To investigate this, we have determined the structure of an unliganded form of HIV-1 RT at 2.35 Å resolution and compared this with our previously refined high-resolution (2.2 Å) structures of RT–NNI complexes[9].

Structure determination

Crystals of unliganded RT were derived from crystals of RT which had been grown as a complex with the NNI HEPT[1] and subjected to our standard cell shrinkage protocol[11], in the absence of HEPT, prior to data collection (Table 1). Initially an incomplete data set to 2.5 Å resolution was collected at room temperature and the 'current best model' for the appropriate cell size (crystal form C, RT–1051U91 complex[9], excluding the NNI), was fitted to the data as nine rigid domains. A difference map indicated unexpectedly large changes in the vicinity of the NNI site; the absence of inhibitor causing a rearrangement of the protein structure. It was concluded that during the cell shrinkage process HEPT had largely diffused out of the crystals. Careful refinement of the structure showed evidence for some residual HEPT at approximately 15 % occupancy. Subsequently, we repeated the protocol for diffusing out the HEPT and collected a full data set to 2.35 Å resolution from a single crystal cooled to 100 K. Although the crystal cell had shrunk further, structure solution was straightforward, and the current *R*-factor is 0.219 (Table 1). In this structure there is no evidence for residual HEPT as can be judged from the omit electron density map for residues in the vicinity of the NNI-binding site (Fig. 1). A further experiment to re-introduce the inhibitor by soaking in HEPT proved successful[9] suggesting that HEPT has a faster off-rate than the tighter binding NNIs[12].

Structure and flexibility

We now have a substantial data base of high resolution structural information on the RT heterodimer. We have apo RT structures in two cell forms (C and E; defined in Table 1), high and medium resolution structures of RT complexes with different NNIs in three cell forms (C and D[9] also E, unpublished results). We have also obtained

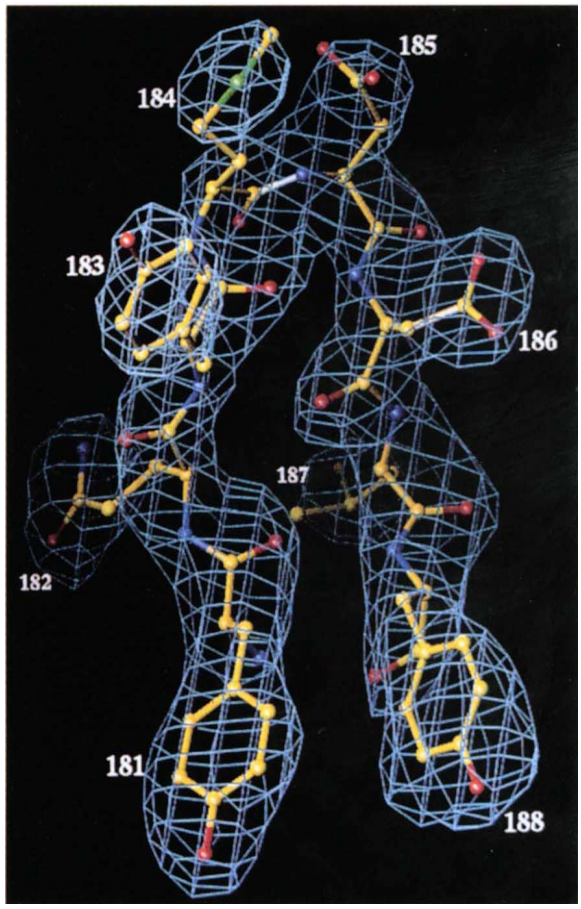

Fig. 1 An omit $|F_{obs}|-|F_{calc}|$ electron density map contoured at a little over 3σ showing well defined density for residues 181–188 of the apo enzyme in crystal form E. The map was calculated using phases from a model produced by omitting these residues and then refining further. The omitted residues are shown in ball-and-stick representation. All nearby electron density is shown, demonstrating the complete absence of bound HEPT in this crystal. Produced using the program O[22].

lower resolution structures (unpublished results) for two further unit cell forms, A (3.7 Å) and B (3.2 Å), which have a higher solvent content[11] than forms C–E. In some cases we have data for the same inhibitor complex in several different cell forms, for instance the RT–1051U91 complex has been studied in forms A, B, C and D. Overall this allows us to assess which structural changes are due to the variations in crystal packing, which are due to the binding of different NNIs, and which are due to the absence of NNIs.

A comparison of the apo RT structures with NNI-bound forms shows changes to be localised primarily in the vicinity of the NNI site (Fig. 2). Away from this site there is a barely significant shift (2.5°) in the relative orientation of the p66 thumb domain. Small shifts in secondary structural elements of the thumb domain in the p51 subunit can also be observed. This leads to the p66 thumb domain moving slightly away from the residues of the polymerase active site in the apo structure. In contrast, much more dramatic domain rearrangements of the p66 fingers and thumb (rotations of up to 20°) occur between different crystal forms. Thus the variation of p66 thumb domain orientation in this family of crystals does not appear to depend critically on the presence, absence or nature of the NNI but rather on the hydration state of the crystal lattice. For current purposes our studies demonstrate that there can be very little energetic drive to major domain rearrangement on transition between apo and drug-bound states. These data do not allow us to comment on possible changes to the range of conformations accessible in going between apo and drug-bound states.

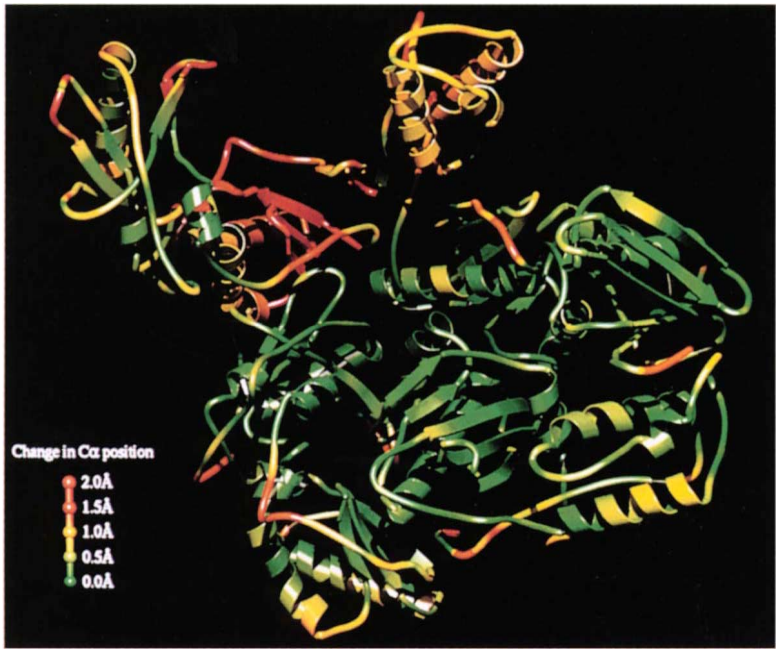

Structure of the p66 polymerase site

The polymerase active sites in both apo structures are well-defined and have very similar conformations (root-mean-square deviation between Cα atoms for 110 residues around the active site is 0.3 Å). The active site conformations observed in the three high-resolution NNI complexes are also similar to each other (r.m.s. deviations on corresponding atoms of 0.4–0.6 Å) but different from that of the apo enzyme (corresponding deviations 1.1–1.2 Å). The conclusions drawn below thus hold for all apo and complex comparisons. Purely for simplicity we use the 100 K apo RT and RT–1051U91 struc-

Fig. 2 A ribbon diagram of the overall structure of the apo RT molecule coloured by structural variation between apo (form C) and drug-bound (RT–1051U91 complex, form C) molecules. Regions coloured green show least variation in Cα position, whilst those in red correspond to changes of 1.6 Å or greater. It can clearly be seen that the most significant changes are largely confined to the p66 palm domain, the site of NNI binding and the polymerase active site. Produced using a version of MOLSCRIPT[23] (modified by R.E.) and rendered with RASTER3D[24].

tures as benchmarks in the following discussion.

The NNI site in p66 is formed between the β7 and β8 hairpin, the strand β4 and the loop containing Leu 100. The most dramatic change on complex formation is the concerted movement of the three strands, β4, β7 and β8, by up to 2.0 Å. These β-strands contain the functional aspartic acid residues 110, 185 and 186 and comprise part of the polymerase active site[9]; the NNIs thus induce a distortion of the active site (Figs 3, 4*a*). In the apo structure there is a solvent inaccessible cavity (volume 360Å^3), situated between the tyrosine residues 181, 183 and 188 and Trp 229. On NNI binding, tyrosines 181, 183, and 188 move to fill this small cavity and a larger cavity is left 'further down' the β-hairpin which accommodates the NNI. The volume of this cavity varies from 620–720 Å^3 in the four inhibitor complexes studied and is connected to bulk solvent by a narrow channel which opens between Lys 101, Val 179 and Glu 138(p51). For strand β4 the conformational change is absorbed several residues beyond the ends of the strand by appropriate coiling and uncoiling of the adjacent helices. Finally, for the three tightly-binding inhibitors, the β-hairpin leading to the thumb domain shows a shift (up to 2.9 Å for His 235–Asp 237) towards the NNI, stabilizing the β9–β11 sheet, as demonstrated by improved electron density compared to the apo structure. In both apo and inhibitor-bound structures the main-chain torsion angles of Met 184 are energetically unfavoured ($\phi \sim 60°$, $\psi \sim -120°$), the peptide being restrained by a hydrogen bond to its carbonyl oxygen. This appears necessary to present both Asp 185 and Asp 186 on the

Table 1 Statistics for crystallographic structure determinations

Data collection details:		
Data collection site	KEK, 1994	SRS, 1994
Wavelength (Å)	0.980	0.870
Collimation (mm)	0.10	0.15
Crystal form	C	E
Number of crystals	2	1
Unit cell (Å)	140.6, 110.9, 73.1	137.5, 109.4, 72.3
Resolution range (Å)	25.0-2.5	25.0–2.35
Observations	141312	369013
Unique reflections	26120	41307
Completeness (%)	64.9	89.5
Reflections with $F/\sigma(F) > 3$	19019	32545
R_{merge} (%)[1]	12.9	8.9
Outer resolution shell:		
Resolution range (Å)	2.6–2.5	2.45–2.35
Unique reflections	1119	3887
Completeness (%)	25.2	73.3
Reflections with $F/\sigma(F) > 3$	279	1790
Refinement statistics:		
Resolution range (Å)	25.0–2.5	25.0–2.35
Unique reflections	26120	41307
R-factor[2]	0.214	0.219
Protein atoms	7943	7943
Water molecules	—	270
r.m.s. bond length deviation (Å)	0.007	0.016
r.m.s. bond angle deviation (°)	1.4	2.0
Mean *B*-factor (Å^2)[3]	55.9/62/—	55/59/51
r.m.s. backbone *B*-factor	3.7	4.4

[1] $R_{merge} = \Sigma |I - \langle I \rangle| / \Sigma \langle I \rangle$
[2] *R*-factor = $\Sigma |F_o - F_c| / \Sigma F_o$
[3] mean *B*-factor for main-chain, side-chain and water atoms, respectively.
[4] r.m.s. deviation between *B*-factors for bonded main-chain atoms.

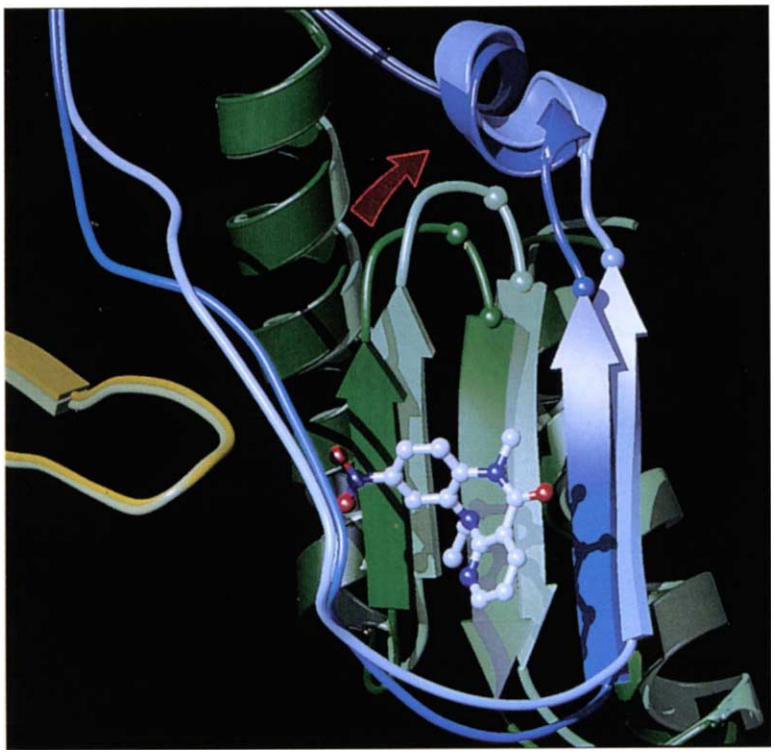

Fig. 3 Comparison of the p66 polymerase active site and the NNI-binding site in the apo enzyme and in the inhibitor-bound form (RT–1051U91) based on a superposition of the two form C models. A ball-and-stick representation is used for the 1051U91 molecule. The apo structure is drawn with more saturated colours and three segments of chain are shown (83–125 in blue, 146–215 in green and 132–152 from the p51 subunit in yellow). Strands β9—β11, which lead into the thumb domain, have been omitted from the diagram for clarity. The three aspartic acid residues contributing to the polymerase active site (110, 185 and 186) are indicated by small balls marking their Cα atoms. The three-stranded β-sheet comprising β4, β7 and β8 moves as a rigid body to create the NNI pocket (the direction of movement is indicated by a red arrow; displacement of Cα for Asp 186 is 1.9 Å), and there is a substantial rearrangement of side chains. There is a large difference from 89–94, this corresponds to a flexible region of the molecule. Produced using a version of MOLSCRIPT[23] (modified by R.E.) and rendered with RASTER3D[24].

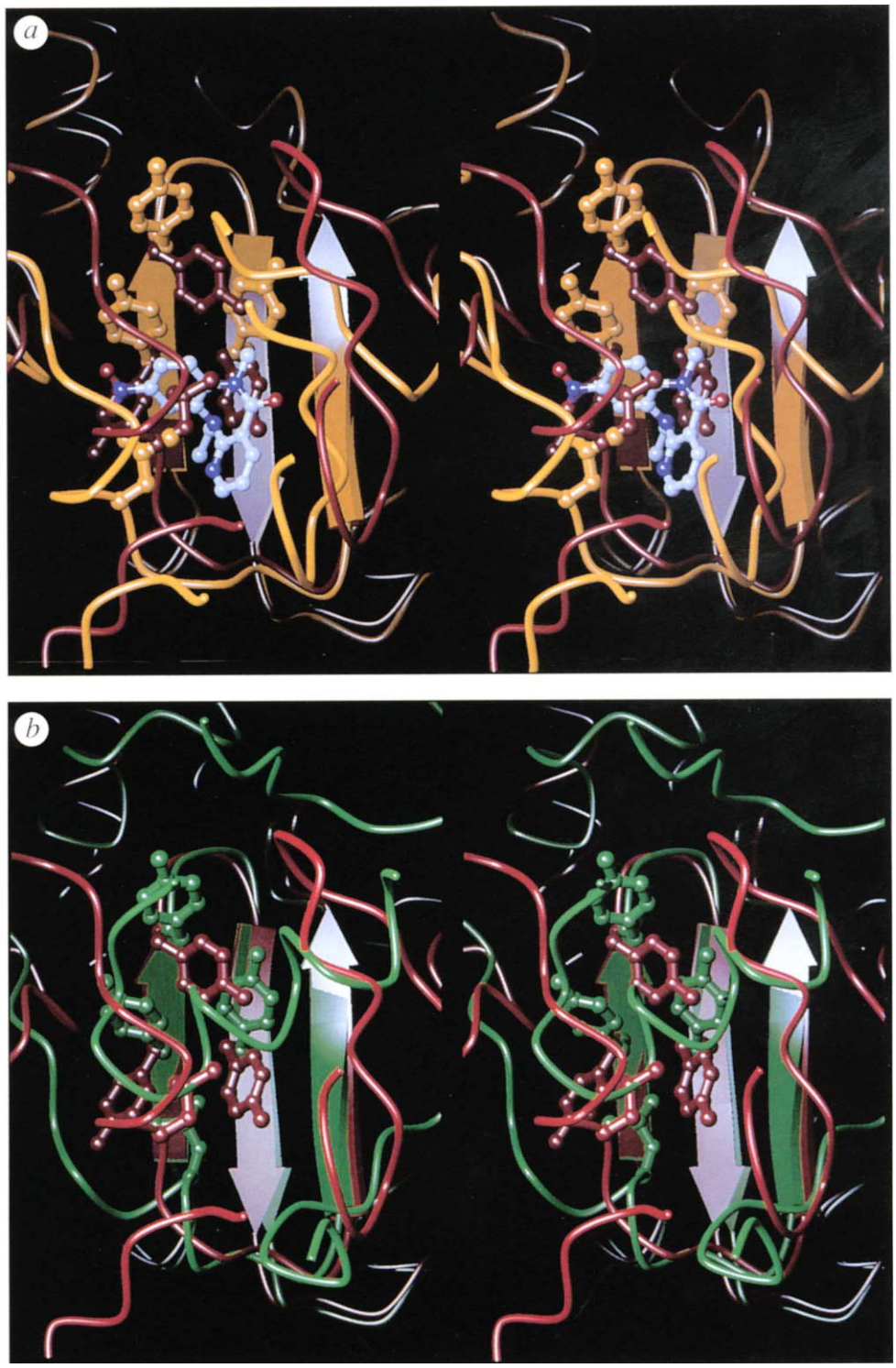

Fig. 4 Stereo views of superpositions of the p66 polymerase active site in the RT–1051U91 complex (orange); the p66 polymerase site in the apo RT structure (red); and the inactive polymerase site in the p51 subunit of the RT–1051U91 complex (green) — there are no significant differences between the p51 polymerase sites in the drug-bound and apo RT models. Note that the superposition is based on the Cα coordinates of strands β4, β7 and β8, the β-sheet that moves as a rigid body on formation of the NNI complex (r.m.s. deviation for the 17 Cα atoms is <0.5 Å in each case), in order to highlight the changes in the environment of the strands containing the catalytic aspartic acid residues. *a*, Comparison of the p66 polymerase sites in the apo RT (red) and RT–1051U91 complex (orange); *b*, comparison of the p66 apo site (red) with the inactive p51 site (green); and *c, next page*, comparison of the p66 site in the RT–1051U91 complex (orange) with the inactive p51 site (green). The 1051U91 is shown as an atom-coloured ball-and-stick representation where appropriate and the side chains of Leu 100 and the tyrosines 181, 183 and 188 are shown in the colours of the relevant model. The similarity between the NNI-bound p66 site and the inactive p51 site is striking, the side chain conformations being particularly similar. The r.m.s. difference for all atoms in residues 174–192 is 1.0 Å between the NNI-bound p66 and inactive p51 sites (for the RT–nevirapine and the RT–α-APA complexes the r.m.s. deviations for the equivalent superpositions are 1.1 Å and 1.3 Å, respectively). By contrast, the corresponding r.m.s. difference between the apo RT p66 site and the RT—1051U91 complex p51 site is 2.1 Å (and 2.2 Å between the apo RT and RT—1051U91 complex). Produced using a version of MOLSCRIPT[23] (modified by R.E.) and rendered with RASTER3D[24].

same face of the β-sheet. In the RT-1051U91 complex the hydrogen-bond donor is provided by Gln 182, whereas in the apo structure Gln 161 provides this interaction and Gln 182 reorients.

On formation of the RT-HEPT complex similar changes in protein conformation are seen to those for the more tightly-binding NNIs. The poor fit of HEPT into the NNI site, however, allows additional flexibility in the side chains of Tyr 181 and Tyr 183, and the β-hairpin from 233–240 retains the conformation of the apo-structure, the hydroxyethoxy substituent of HEPT restricting any change.

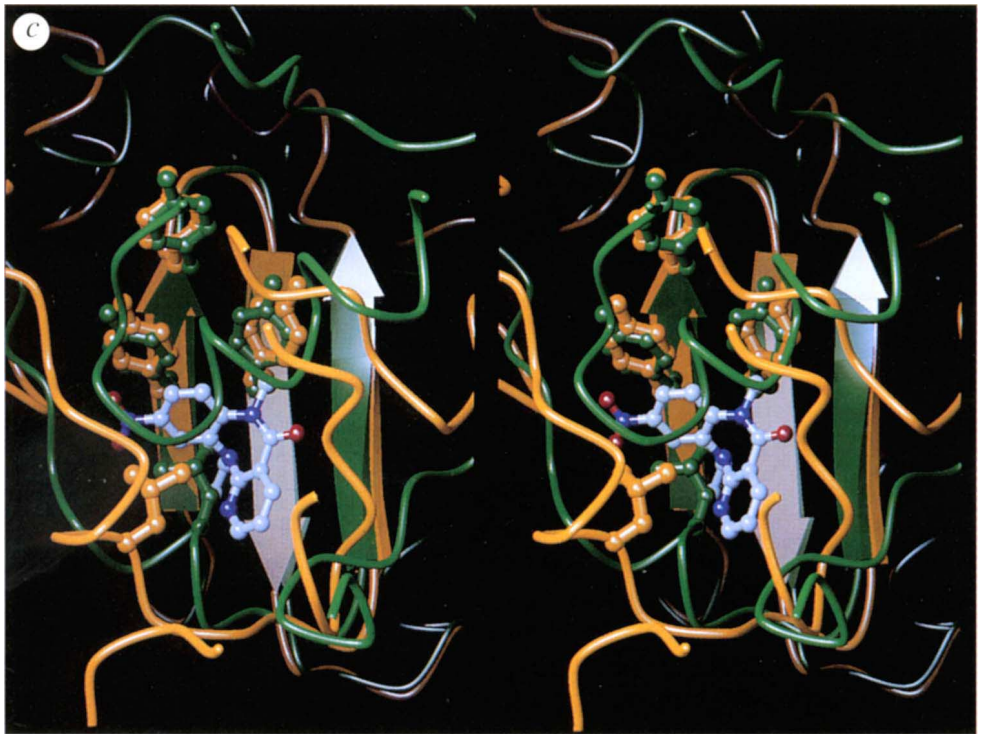

Comparison of the p66 and p51 polymerase sites

The p51 chain of the RT heterodimer contains an inactive polymerase site, which can be compared with the p66 site in the apo RT and RT–1051U91 complex (Figs 4*b,c*). The superposition is based on the Cα atoms of the β7–β8 hairpin and can be compared with Fig. 4*a*. Whilst the environment of the hairpin clearly varies between the apo RT p66 site, the RT–1051U91 complex p66 site and the inactive p51 site in the RT–1051U91 complex, there is a striking similarity between the actual conformations of the hairpin in the drug-bound p66 conformation and in its inactive p51 counterpart. This is especially true of the side-chain conformations and the comparison holds for all three tightly-binding NNI complexes. The RT–HEPT complex, an outlier to the general pattern, shows alternate conformations for some of these side chains[9]. Investigation of complexes of RT with more tightly-binding HEPT analogues is required to establish if these features are responsible for the relatively low affinity of HEPT. Extending the analogy between the drug-bound p66 site and the inactive p51 site, the side chain of Leu 100 in p51 occupies a similar position to the ethyl group of 1051U91 (and the cyclopropyl group of nevirapine), and the rest of the NNI has a similar position to helix α10 (residues 364–383). NNI binding thus moulds the polymerase active site into the conformation observed in the inactive p51 chain. The unusual Met 184 conformation, seen in both apo and drug-bound p66 chains is also present in the p51 chain, retained by a hydrogen bond to Tyr 115 (situated in a short 3_{10}-helix connecting the p51 fingers and palm).

Mechanism of inhibition

These data provide insight into the mechanism of NNI action. We observe two distinct conformations for the p66 polymerase site: one in the drug-bound structures[9] and in the p51 site (where the polypeptide chain fulfills a similar role to the NNIs), the other in the apo structure. The orientation of the p66 thumb is very similar in the liganded and unliganded RT structures and the change observed in the conformation of the β-sheet leading to the thumb on binding of 1051U91, nevirapine and α-APA is not seen with the HEPT complex; arguing against the 'molecular arthritis' model for NNI action[7]. Instead the effects of the NNIs are localized to an essentially rigid-body movement of the sheet comprising β4, β7 and β8, suggesting that the repositioning of the catalytic aspartic acids within the polymerase site as a whole is sufficient to cause inhibition. Alternatively, the catalytic cycle may require the ability to adopt both the 'apo' and 'drug-bound' conformations; which is in our view less likely. These models are in-line with recent reports that DNA binding to RT is not perturbed by bound NNIs, and may actually be enhanced by their presence[13,14].

This direct comparison of apo and NNI-bound RT structures in similar crystal forms delineates the conformational changes required to form the NNI site. It reveals that the NNIs achieve specificity not simply by filling an arbitrary pocket but rather by emulating the protein–protein interactions that stabilize the structure of the inactive p51, resulting in a distortion of the polymerase active-site by movement of the key aspartic acid residues, and hence a common mechanism of inhibition by this diverse class of HIV-1 specific RT inhibitors.

Note added in proof: After submission of our manuscript a study of the pre-steady state kinetics of NNI inhibition of HIV-1 RT has been reported[25]. In this work the authors conclude that there is direct communication between the NNI and catalytic sites. They suggest as plausible the possibility that the binding of NNIs alters the position of the aspartate carboxyl groups slowing the rate of chemical reaction. It is also shown that the NNI does not significantly alter the rate or equilibrium constant for conformational change of the enzyme during the catalytic cycle. These results are therefore in complete agreement with our structural studies.

Methods

Crystallographic data collection. As detailed previously[11] orthorhombic crystals (space group $P2_12_12_1$) of the RT–HEPT complex were grown at 4 °C by equilibration against reservoirs of 6 % PEG 3400 and citrate/phosphate at pH 5.0 using sitting drops. Crystallisation required macroscopic seeding. These crystals were then subjected to partial dehydration by equilibration with 46 % PEG 3400 over a period of 3 days prior to data collection, this increased the order in the crystals (allowing higher resolution data to be collected), removed the

Acknowledgements
We are grateful to A. Nakagawa and N. Sakabe at the Photon Factory, Japan, and staff at SRS, Daresbury, UK, for their help with X-ray data collection; B. Willcox and A. Hopkins for their key role in collecting the SRS data and, with E. Garman, in developing the cooling protocols; R. Bryan for computing facilities and S. Lee for help with the preparation of figures. This work has received long-term support from the MRC AIDS Directed Programme. The Oxford Centre for Molecular Sciences is supported by the BBSRC and MRC. EYJ is supported by a Royal Society University Research Fellowship. Atomic co-ordinates for the apo RT have been deposited with the Protein Data Bank, Brookhaven National Laboratory, USA, for release one year after publication.

inhibitor HEPT and allowed the crystals to be flash cooled. X-ray data from crystal form C were collected on BL-6A2 at the Photon Factory, KEK, Japan (see ref. 9) by the Weissenberg method[15,16]. A crystal-to-detector distance of 429.7 mm, coupling constant of 1.5 ° mm^{-1}, oscillation range of 3.5 ° and exposure time of 140 s were employed. Data were collected at 14 °C. Diffraction data from crystal form E were collected on Station 9.6 at the SRS, Daresbury Laboratory, UK by the oscillation method using a 30 cm MAR imaging plate. A crystal-to-detector distance of 380.0 mm and oscillation range of 1.5° were employed. The crystal was flash cooled to 100 K, which allowed 86 data images to be collected from one crystal. The low temperature led to a further reduction of the unit cell volume by about 5 %. Autoindexing and data processing of both data sets were performed with DENZO[17].

Structure determination protocol. A model of RT–1051U91 in a similar unit cell (form C, excluding water and inhibitor molecules) was refined against the form C apo data, initially from 8.0–4.0 Å treating it as a single rigid body (*R*-factor = 0.264), and then against 8.0–2.5 Å data, treating each domain as a rigid group (*R*-factor = 0.304, program X-PLOR[18]). An $|F_{obs}|-|F_{calc}|$ difference map phased from this model showed major local structural changes in the palm domain of p66 resulting from the loss of the HEPT molecule, but little change elsewhere. The model was rebuilt based on a $2|F_{obs}|-|F_{calc}|$ electron density map using the program FRODO[19] on an Evans and Sutherland ESV workstation. The resulting model was then subjected to simulated annealing[20] and restrained individual temperature factor refinement. Due to the incompleteness of data, atoms distant from the NNI-binding site (defined as atoms more than 25 Å from the C_α of Tyr 188) were tightly restrained to their position in the drug-bound structure and strong stereochemical restraints were employed. Residual electron density around the side chain of Tyr 188 suggested that the inhibitor was not completely excluded from the NNI-binding site. Further rounds of careful refinement (with a bulk solvent correction) and model rebuilding aided by inspection of 3.0 Å resolution, occupancy corrected, maps followed. Occupancy correction used the RT–HEPT model, suitably positioned in the unit cell, at an occupancy of 0.15 as a partial structure. The apo RT model, with an occupancy of 0.85, was then refined against the X-ray data combined with the above set of partial-structure factors.

The orientation and position of the RT molecule in the unit cell of crystal form E were determined using the above apo RT model and data in the resolution range 15.0–6.0 Å, first by Patterson Correlation refinement[21] treating the model sequentially as 1, 2 and 9 rigid groups according to subunit and domain organisations of the molecule and then translation search around the origin, followed by rigid-body refinement with X-PLOR. Several rounds of full refinement and model rebuilding produced the current form E model. This model, superposed domain-wise onto the initial model and refined against the data of crystal form C, resulted in the present form C apo model.

Received 11 January; accepted 22 February 1995.

1. Baba, M. *et al.* Highly specific inhibition of human immunodeficiency virus type-1 by a novel 6-substituted acyclouridine derivative. *Biochem. biophys. Res. Commun.* **165**, 1375–1381 (1989).
2. Pauwels, R. *et al.* Potent and selective inhibition of HIV-1 replication in vitro by a novel series of TIBO derivatives. *Nature* **343**, 470–474 (1990).
3. Merluzzi, V.J. *et al.* Inhibition of HIV-1 replication by a nonnucleoside reverse transcriptase inhibitor. *Science* **250**, 1411–1413 (1990).
4. De Clercq, E. HIV-1-specific RT inhibitors: highly selective inhibitors of human immunodeficiency virus type 1 that are specifically targeted at the viral reverse transcriptase. *Med. Res. Rev.* **13**, 229–258 (1993).
5. Wu, J.C *et al.* A novel dipyridodiazepinone inhibitor of HIV-1 reverse transcriptase acts through a non-substrate binding site. *Biochemistry* **30**, 2022–2026 (1991).
6. Debyser, Z. *et al.* An antiviral target on reverse transcriptase of human immunodeficiency virus type 1 revealed by tetrahydroimidazo-[4,5 1-jk][1,4] benzodiazepin-2(1H)-one and -thione derivatives. *Proc. natn. Acad. Sci. U.S.A.* **88**, 1451–1455 (1991).
7. Kohlstaedt, L.A., Wang, J., Friedman, J.M., Rice, P.A. & Steitz, T.A. Crystal structure at 3.5 Å resolution of HIV-1 reverse transcriptase complexed with an inhibitor. *Science* **256**, 1783–1790 (1992).
8. Smerdon, S.J. *et al.* Structure of the binding site for nonnucleoside inhibitors of the reverse transcriptase of human immunodeficency virus type 1. *Proc. natn. Acad. Sci. U.S.A.* **91**, 3911–3915 (1994).
9. Ren, J. S. *et al.* High resolution structure of HIV-1 RT: insights from four RT-inhibitor complexes. *Nature struct. Biol.* **2**, 293–302 (1995).
10. Tantillo, C. *et al.* Locations of anti-AIDS drug binding sites and resistance mutations in the three-dimensional structure of HIV-1 reverse transcriptase. *J. molec. Biol.* **243**, 369–387 (1994).
11. Stammers, D.K. *et al.* Crystals of HIV-1 reverse transcriptase diffracting to 2.2 Å resolution. *J. molec. Biol.* **242**, 586–588 (1994).
12. Debyser, Z. *et al.* Allosteric inhibition of human immunodeficiency virus type 1 reverse transcriptase by tetrahydroimidazo[4,5,1-jk][1,4]benzodiazepin-2(1H)-one and -thione compounds. *Molec. Pharmacol.* **41**, 203–208 (1992).
13. Bakhanashvili, M. & Hizi, A. Interaction of the reverse transcriptase of human immunodeficiency virus type 1 with DNA. *Biochemistry* **33**, 12222–12228 (1994).
14. Divita, G. *et al.* Kinetics of interaction of HIV reverse transcriptase with primer/template. *Biochemistry* **32**, 7966–7971 (1993).
15. Sakabe, N. X-ray diffraction data collection system for modern protein crystallography with a Weissenberg camera and an imaging plate using synchrotron radiation. *Nucl. Instr. Meths phys. Res.* **303**, 448–463 (1991).
16. Stuart, D.I. & Jones, E.Y. Weissenberg data collection for macromolecular crystallography. *Curr. Opin. struct. Biol.* **3**, 737–740 (1993).
17. Otwinowski, Z., Oscillation data reduction program, in *Data collection and Processing* (L. Sawyer, N. Isaacs, S. Bailey, Eds.) pp. 56-62 (SERC Daresbury Laboratory, Warrington, England, 1993).
18. Brünger, A.T., *X-PLOR Manual V. 3.1.* (Yale University, New Haven, CT; 1992).
19. Jones, T.A. Interactive computer graphics: FRODO. *Meths. Enzymol.* **115**, 157–171 (1985).
20. Brünger, A.T., Krukowski, A. & Erickson, J. Slow-cooling protocols for crystallographic refinement by simulated annealing. *Acta crystallogr.* **A46**, 585–593 (1990).
21. Brünger, A. T. Extension of molecular replacement: a new search strategy based on Patterson correlation coefficient refinement. *Acta crystallogr.* **A46**, 46–57 (1990).
22. Jones, T.A., Zou, J.Y., Cowan, S.W. & Kjeldgaard, M. Improved methods for building protein models in electron density maps and the location of errors in these models. *Acta crystallogr.* **A47**, 110–119 (1991).
23. Kraulis, P.J. MOLSCRIPT: a program to produce both detailed and schematic plots of protein structures. *J. appl. Crystallogr.* **24**, 946–950 (1991).
24. Merritt, E.A. & Murphy, M.E.P. Raster3D version 2.0. A program for photorealistic molecular graphics. *Acta crystallogr.* **D50**, 869–873 (1994).
25. R.A. Spence, W.M. Kati, K.S. Anderson & K.A. Johnson *Science* **267**, 988–993(1995).